RESEARCH ARTICLE
SPACE PHYSICS

Earth and Planetary Physics
10: 156–166, 2026
doi: 10.26464/epp2026015

Simultaneous lidar observations of the sporadic Ni layer and sporadic Na layer in the MLT

ZhiJun Zhao[1], XuYang Jiang[1], FuJu Wu[1,2*], YuHang Qi[1], Jing Jiao[2], and GuoTao Yang[2]

[1]School of Physics, Henan Normal University, Xinxiang Henan 453000, China;

[2]State Key Laboratory of Solar Activity and Space Weather, Beijing 100190, China

Key Points:

- Synchronized observations of sporadic Ni and sporadic Na layers were conducted using a Na–Ni dual-wavelength lidar system.
- The seasonal variation of sporadic Ni is similar to that of sporadic Na.
- The peak density ratio of sporadic Na to sporadic Ni is approximately 5, which is half the density ratio of the two main layers.

Citation: Zhao, Z. J., Jiang, X. Y., Wu, F. J., Qi, Y. H., Jiao, J., and Yang, G. T. (2026). Simultaneous lidar observations of the sporadic Ni layer and sporadic Na layer in the MLT. *Earth Planet. Phys.*, *10*(1), 156–166. http://doi.org/10.26464/epp2026015

Abstract: Here we report on simultaneous lidar observations of sporadic Ni (Nis) layers and sporadic Na (Nas) layers in the atmosphere over Yanqing, Beijing (40.42°N, 116.02°E) from April 2019 to October 2022. During 343 nights of observation, 68 Nis and 56 Nas were observed. The seasonal variation of Nis and Nas was also obtained, with the highest occurrence of Nis being in July (43%) and that of Nas being in June (61%). We found that the seasonal variation of Nis is similar to that of Nas and that both occur more frequently in summer than in winter. In addition, we found 23 events in which Nis and Nas occur simultaneously. The average peak altitude of Nas is approximately 1 km higher than that of Nis, and the peak density ratio of Nas to Nis is approximately 5, which is half the density ratio of the two main layers. Additionally, the strength factor for Nas is smaller than that for Nis. Through data analysis of sporadic E layers (Es), we found that Nis and Nas has a significant correlation with Es. The neutralization rates of Ni^+/Na^+ were calculated according to the dissociative recombination reaction of Ni^+/Na^+ and the WACCM-Ni (Whole Atmosphere Community Climate Model of Ni). The production rates of Ni and Na were estimated to be approximately 1:4.4, which is consistent with the density ratio of Nis to Nas. The results showed that the neutralization reaction of Ni^+, Na^+, and electrons in Es is the main reason for the formation of the Nis layer and the Nas layer.

Keywords: lidar observation; sporadic Ni layer; sporadic Na layer; sporadic E layer; seasonal variation

1. Introduction

The atmospheric metal layer located at 80–105 km originates from the ablation of meteors (Plane et al., 2015). When meteors enter the Earth's atmosphere at a high speed, metal elements such as Na, K, Fe, Ca, Ca^+ are released to form the atmospheric metal layer caused by frictional heating. The atmospheric metal layer is a good tracer for studying the dynamics and photochemical processes of the middle and upper atmosphere (Cai XG et al., 2017; Yuan T et al., 2021).

Lidar is a powerful tool for detecting the atmospheric metal layer because of its high detection accuracy and spatiotemporal resolution. In 1969, Bowman et al. successfully detected the Na layer for the first time by using Na resonance fluorescence lidar (Bowman et al., 1969). Lidar detection of the Na, K, Fe, and Ca layers has been extensively studied around the world (Gardner et al., 2011; Raizada et al., 2011; Wang ZL et al., 2017; Raizada et al., 2020). The average characteristics of the atmospheric metal layer, such as seasonal variations and diurnal variations, have also been reported (Xia Y et al., 2020; Hu YJ and Yi F, 2021; Xun YC et al., 2024; Wu Fang et al., 2025). With the development of lidar technology, some special phenomena of the atmospheric metal layer have gradually been observed. The sporadic metal layer is the most significant phenomenon of the atmospheric metal layer on a short time scale.

The sporadic Na (Nas) layer was the first sporadic phenomenon to be discovered in the atmospheric metal layer region. For the first time, Clemesha et al. (1978) detected that Na density increases rapidly in a very short period of time (about 5 min) within a very narrow height range. Subsequently, more Nas layers were observed by lidar from low to high latitudes (Dou XK et al., 2013; Jiao J et al., 2014; Ma Z et al., 2014; Yuan T et al., 2014; Qiu SC et al., 2016; Zhang TM et al., 2017; He SM et al., 2025). It was found, based on the researchers' observations, that Nas layers usually last for tens of minutes or hours and that their peak density is approximately 2–5 times that of the background Na density (Qiu SC et al., 2016). In addition, researchers have reported that the frequency of Nas is highest during June and July and lowest in January and February. This variation indicates that Nas events occur with

First author: Z. J. Zhao, zhaozhijun@htu.edu.cn
Correspondence to: F. J. Wu, wufuju@htu.edu.cn
Received 28 MAY 2025; Accepted 11 OCT 2025.
First Published online 14 NOV 2025.

significantly higher frequency in summer than in winter (Yi F et al., 2002; Jiao J et al., 2015). The formation of Nas layers is related to many factors, such as meteor injection, atmospheric temperature, and ion transformation (Von Zahn et al., 1987; Yi F et al., 2007; Takahashi et al., 2015; Qiu SC et al., 2018, 2021, 2023). Because of the very good correlation between Na and the sporadic E layer (Es), researchers have gradually accepted the theory that Na^+ within Es in the low-E region are reduced to Na atoms through a series of reactions (Cox and Plane, 1998; Jiao J et al., 2015).

Nickel is one of the more challenging atoms in the middle and upper atmosphere because of its low abundance and relatively small backscattering cross section (i.e., 6–30 times lower than that of the Na atom; Wu FJ et al., 2021). In 2015, Collins et al. first observed Ni layers in Chatanika, Alaska (65°N, 147°W) and concluded that the Ni density is ~16,000 cm^{-3} (Collins et al., 2015). Gerding et al. (2019) then conducted six nights of lidar observation of Ni layers over Kühlungsborn (54°N, 12°E) in Germany and found that the density of the Ni layers is ~280–450 cm^{-3}. Such a large difference in detection results is obviously inconsistent with the origin mechanism of the atmospheric metal layer. To solve the Ni density problem, Wu FJ et al. (2021) used high-detection precision Ni lidar at the Yanqing station (40.41°N, 116.01°E) to detect the Ni layers, and they calculated the Ni density over 25 nights. The results showed that the Ni peak density ranges from 98 to 460 cm^{-3} and that the average peak density is 258 ± 115 cm^{-3}. This finding is in good agreement with the earlier results obtained by Gerding et al. (2019) at Kühlungsborn. The Ni lidar and Na lidar at the Yanqing station (40.41°N, 116.01°E) were established based on a dual-wavelength lidar system, which allows the simultaneous lidar detection of Ni and Na. From 2019 to the present, the dual-wavelength lidar has been operating steadily and has accumulated sufficient data. By analyzing the lidar data, Jiao J et al. (2022) found that the main Ni and Na layers peak around 85 and 92 km, respectively, and that the density ratio of Ni to Na is approximately 1:10. It is notable that Wu FJ et al. (2022) reported the thermosphere–ionosphere sporadic Ni (TISNi). The thermosphere–ionosphere sporadic metal layer refers to the phenomenon of a special metal layer that occurs within a height range of 105–120 km that is significantly separated from the main metal layer (80–105 km) and is closely related to Es. Wu FJ et al. (2022) also discovered that the TISNi and thermosphere–ionosphere sporadic Na (TISNa) layers show close correlations. It is important that the density ratio of TISNi to TISNa is close to 1, which is approximately 10 times the density ratio of Ni to Na in the main layer. This ratio indicates Ni enrichment in the thermosphere–ionosphere region. By combining the comparative analysis of Es data and the Whole Atmosphere Community Climate Model for Ni (WACCM-Ni), Wu FJ et al. (2022) concluded that direct recombination of Ni^+/Na^+ with electrons produces thermosphere–ionosphere Nis and Nas. Nickel is known to be a metal atom that is rarely detected; thus, the study of this special phenomenon contributes to a better understanding of the formation of the atmospheric metal layers.

However, the Nis phenomenon in the main metal layer (80–105 km) has not been statistically analyzed. Its seasonal variation, density, and correlation with sporadic phenomena in other metal layers remain unknown. Therefore, we utilize the dual-wavelength lidar data from the Yanqing station to statistically screen out Nis and compare it with Nas for analysis. We study the density, seasonal variations, and characteristic parameters of the two, providing a new research perspective for the study of sporadic metal layers in the main layer.

In this article, we present a comprehensive statistical analysis of lidar data observed from April 2019 to October 2022 over 343 nights, or 3145 h. The characteristic parameters of Nis and Nas and their seasonal variations are described. The characteristics of the Nis layer are compared with those of the Nas layer observed at the same time, and the Nis and Nas layers are compared with the Es layer detected in the ionosphere. Section 2 briefly introduces the lidar system and data processing methods, and the lidar observations are described in Section 3. Finally, the discussion and conclusion are presented in Sections 4 and 5, respectively.

2. The Lidar System and Data Processing

2.1 The Lidar System

The lidar used to measure the Ni layer and the Na layer at the same time is a dual-wavelength lidar system at the Yanqing station (40°N, 116°E). The entire system includes four parts: a transmitter, a receiver, a data acquisition component, and an automatic control. As shown in Figure 1, two pulsed dye lasers for the detection of the Na and Ni layers are pumped by a pulsed Nd:YAG (yttrium aluminum garnet) base beam. One of the dye lasers excites Na resonance fluorescence transitions at 589 nm (Jiao J et al., 2022). Another dye laser generates a laser beam at a

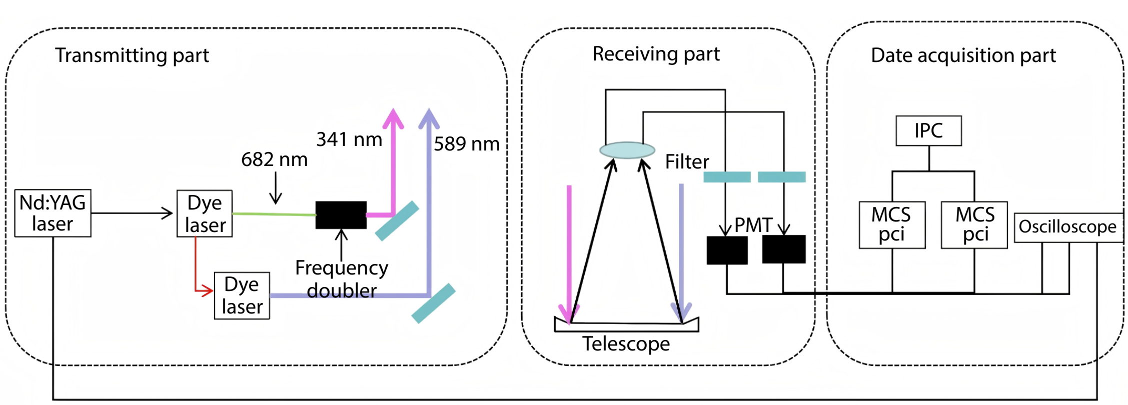

Figure 1. Schematic diagram of the dual Na–Ni lidar system.

wavelength of 682 nm. This beam is then directed into a frequency doubler, producing 341 nm laser light for the detection of Ni atoms (Wu FJ et al., 2021). The receiver uses a 1230-mm-diameter reflector telescope to receive backscattered photons from the atmosphere. In terms of data acquisition, a photon-counting-based multichannel scaler (MCS-PCI) is used to obtain time-resolved data. Raw data files are stored at 96 m spatial resolution and 33 s temporal resolution. The lidar system parameters are shown in Table 1.

Table 1. Parameters of the Na–Ni lidar system.

Parameter	Ni	Na
Transmitter		
Wavelength	341 nm	589 nm
Pulse energy	17 mJ	40 mJ
Line width	0.9574 GHz	1.473 GHz
Repetition rate	30 Hz	30 Hz
Beam divergence	0.21 mrad	<0.5 mrad
Receiver		
Telescope diameter	1.23 m	1.23 m
Field of view	0.625 mrad	0.625 mrad
Data acquisition		
Temporal resolution	33 s	33 s
Vertical spatial resolution	96 m	96 m

2.2 Data Processing

First, we calculate the Ni or Na density at altitude z by using the standard lidar equations:

$$n_{Mt}(z) = n_A(z_R)\frac{N_{Mt}(z) - N_B z^2}{N_R(z_R) - N_B z_R^2}\frac{\sigma_r}{\sigma_{\text{eff}}},$$

where Mt = Ni or Na, $n_{Mt}(z)$ is the density of Ni or Na; $n_A(z_R)$ is the total atmospheric density at the reference altitude, given by the NRLMSISE-00 (U.S. Naval Research Laboratory Mass Spectrometer and Incoherent Scatter Radar) model (Chu XZ and Papen, 2005); N_{Mt} and N_R are the number of echo photons received by the telescope at altitude z and reference altitude z_R, respectively; N_B is the background noise, and the background noise of Ni is the sum of the altitude-independent PMT (photomultiplier tube) dark count rate and stray light signal and the altitude-dependent Rayleigh background signal superimposed on the resonance signal. The altitude of the background noise is 130–150 km; the reference altitude z_R of the Ni/Na layer is 35–40 km; σ_r is the Rayleigh backscatter cross section at reference altitude z_R; and σ_{eff} is the effective backscatter scattering cross section. For Ni atoms, $\sigma_r = 3.55 \times 10^{-31}\text{m}^2/\text{sr}$, $\sigma_{\text{eff}} = 1.58 \times 10^{-17}\text{m}^2/\text{sr}$, and for Na atoms, $\sigma_r = 4.14 \times 10^{-32}\text{m}^2/\text{sr}$, $\sigma_{\text{eff}} = 5.22 \times 10^{-16}\text{m}^2/\text{sr}$.

The lidar system collected high signal-to-noise ratio data for approximately 343 nights and 3145 h over nearly 3 years of observation. Figure 2 presents the monthly statistics of observation hours and nights, with data from different years combined into a single year based on the number of observation days. Because of the higher rainfall in the Beijing area during summer, the observation time was substantially reduced in this season. Using the collected data, we selected Nis and Nas based on the following criteria:

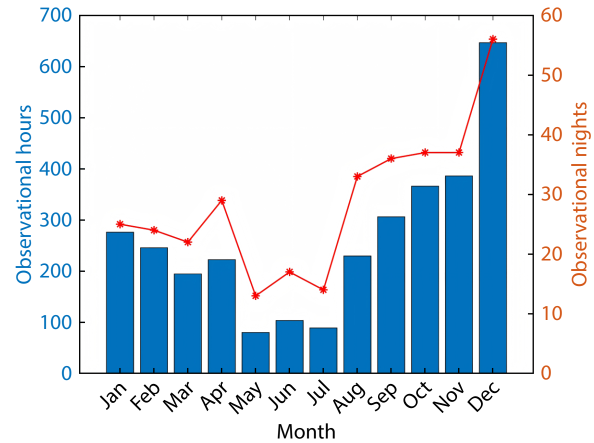

Figure 2. Statistics on the observational hours and nights of lidar in each month.

(1) The maximum peak density of the Nis and Nas layer must be at least twice the density of the background Ni/Na layer at the same altitude (i.e., a strength factor ≥2, defined as the maximum peak density of the Nis and Nas divided by the average density of the background metal layer at the same height);

(2) The Nis and Nas must persist for more than half an hour; and

(3) The maximum peak density of the Nis and Nas must exceed half the peak density of the main Ni/Na layer at the same time.

Applying these constraints, we identified 68 Nis and 56 Nas. It is worth noting that the density of the main Na layer is relatively high, causing the strength factor of some Nas to be low or for their peak density to be less than half the main Na layer peak density. As a result, these Nas failed to meet the established criteria. For this reason, the number of Nas we recorded was lower than the number of Nis.

3. Observational Results

3.1 Seasonal Variations in the Nis and Nas Layers

Figure 3 shows the density variations of the Ni and Na layers on May 28, 2019, along with their respective profiles at maximum density for the Nis and Nas. The temporal and spatial resolutions are 15 min and 96 m, respectively. Sporadic Ni and sporadic Na appeared at similar heights at the same time. The Nis peak density reached its maximum value at 15:00 universal time (UT; ~245.154 cm^{-3}), as shown in Figure 3b. However, the Nas peak density reached its maximum (1949.49 cm^{-3}) at 13:45 UT, as shown in Figure 3d. This occurred approximately 1.15 h earlier than the time at which the Nis reach its peak density, and the Nas peak density was 8 times higher than that of Nis. This is a typical example of the simultaneous occurrence of Nis and Nas layers observed in the lidar data.

To better illustrate the seasonal variations of Nis and Nas, Figure 4

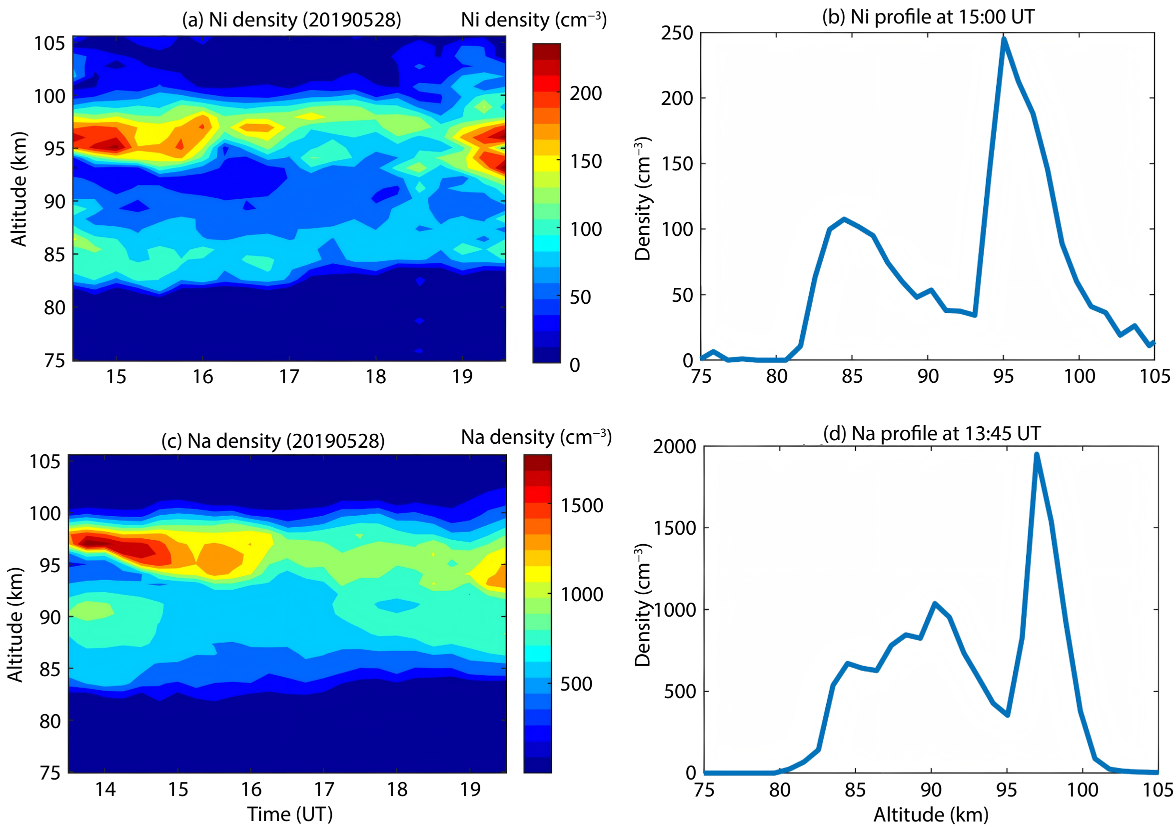

Figure 3. (a) Contour of the Ni layer observed on May 28, 2019, and (b) profile of the Ni density observed at 15:00 UT. (c) Contour of the Na layer observed on May 28, 2019, and (d) profile of the Na density observed at 13:45 UT.

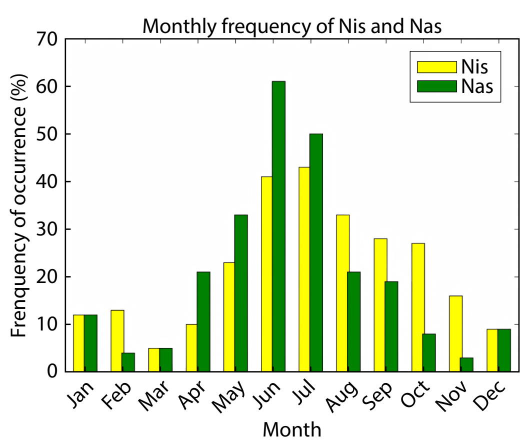

Figure 4. Seasonal variations of Nis and Nas.

presents a comparative analysis. The results clearly show that Nis peaks in July with a frequency of 43%, whereas Nas exhibits maximum occurrence in June at 61%. Both Nis and Nas occur more frequently in summer and less frequently in winter, which aligns with previous Nas studies (Jiao J et al., 2015, 2022; Qiu SC et al., 2016). However, distinct differences exist between Nis and Nas. As shown in Figure 4, except for February, Nas consistently demonstrates a higher occurrence rate than Nis until August. However, from August onward, the frequency of Nas becomes lower than that of Nis. This shift may be attributed to seasonal variations in the main Na layer density. The peak density of the main Na layer increases during the fall and winter months, and some Nas do not meet the selection criterion that their peak density must be half the peak density of the main Na layer, resulting in the situation described above.

We conducted a comprehensive analysis of 68 Nis and 56 Nas and identified 23 cases of co-occurring Nis and Nas layers. Figure 5 displays the monthly distribution of these simultaneous events. The figure clearly shows that in June and July, the frequency of simultaneous occurrence of Nis and Nas is the highest, with a total of 10 nights. This number is followed by August and September (8 nights), whereas April, October, and December show the lowest frequency of co-occurrence, with only 1 night of simultaneous events recorded for each of these months. Further, from the

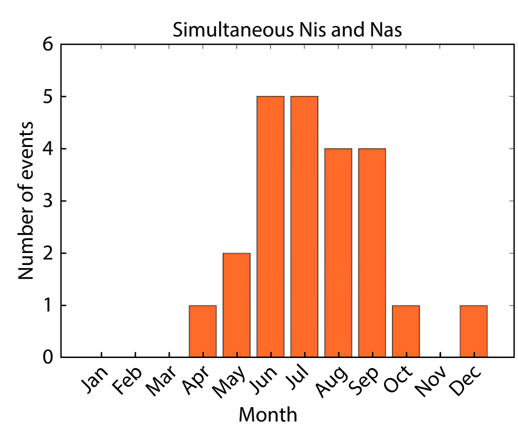

Figure 5. Simultaneous Nis and Nas.

seasonal perspective, the number of simultaneous Nis and Nas in summer is significantly higher than in winter. It is worth noting that no simultaneous occurrence of Nis and Nas was observed in January, February, March, and November. This seasonal absence may be associated with variations in mesopause temperature, chemical reactions, and dynamic processes. Within the main layer range of the metal layer, the density of Na is highly correlated with temperature, which mainly results from the influence of oxygen atom and hydrogen atom chemistry on the distribution relationship of Na between atomic sodium and its main storage form, $NaHCO_3$ (Plane et al., 1999). In fact, the mesopause temperature at mid-latitudes in the northern hemisphere is generally higher in winter than in summer. Higher temperatures enhance neutral chemical reactions, increasing the production of background metal atoms in the main layer. The chemical reactions are shown in Table 2.

This elevated background density can suppress the identification of sporadic layers because the relative contrast between the sporadic and background layers becomes weaker. As a result, many Nas in January, February, and November did not meet our screening criteria. Coupled with the limited number of observations in March, this explains why simultaneous Nis and Nas were not observed in the winter months. Additionally, other factors, such as dynamic processes, may contribute to this phenomenon, although consideration of these processes is beyond the scope of this article. We will continue to collect more data in follow-up work and conduct further research.

Table 2. The neutral chemical reaction of Na.

Reaction	Rate coefficient[a]
$NaO + O \rightarrow Na + O_2$	$(2.2 \times 10^{-10})(T/200)^{1/2}$
$NaHCO_3 + H \rightarrow Na + H_2CO_3$	$(1.84 \times 10^{-13})T^{0.777}\exp(-1014/T)$

[a] Units for bimolecular reactions: cubic centimeters per molecule per second. *T* is temperature.

3.2 Characteristic Parameters of the Simultaneous Nis and Nas

We conducted a detailed statistical analysis of the main parameters of 23 simultaneous Nis and Nas to investigate their potential interrelationships and distinguishing characteristics. Figure 6 systematically presents critical parameters of Nis and Nas, including the peak altitude, duration, time of occurrence, and peak time. The upper row (green bars) displays Nis parameters, whereas the lower row (purple bars) corresponds to Nas parameters.

Figures 6a and 6b display the peak altitude distributions: both Nis and Nas layers appear above 95 km, with Nis predominantly occurring between 96 and 97 km, whereas Nas are typically observed approximately 1 km higher, at 97–98 km. Figures 6c and 6d show the distributions of Nis and Nas durations. The data revealed that 16 Nis and 18 Nas persisted for more than 2 h. Sporadic Ni shows the maximum frequency within the 3–4 h range, whereas Nas is predominantly concentrated in the 2–3 h range. Figures 6e and 6f show the distribution of occurrence times, with the Nis exhibiting a maximum between 22:00 and 00:00 local time (LT) and the Nas exhibiting a broader maximum between 20:00 and 00:00 LT. The peak times in Figures 6g and 6h show that the maxima for both the Nis and Nas layers occur between 00:00 and 02:00 LT. In summary, although the characteristic parameters of Nis and Nas show small differences, their overall trends are similar, which indicates good correlation between Nis and Nas.

Figure 7 presents a comparative analysis of peak density and strength factors between Nis and Nas. The upper row (blue bars) displays statistical data for Nis, whereas the lower row (pink bars) shows Nas parameters. Specifically, Figures 7a and 7b demonstrate the peak density distributions for Nis and Nas, respectively. The statistical analysis showed that the peak density of Nis has a maxi-

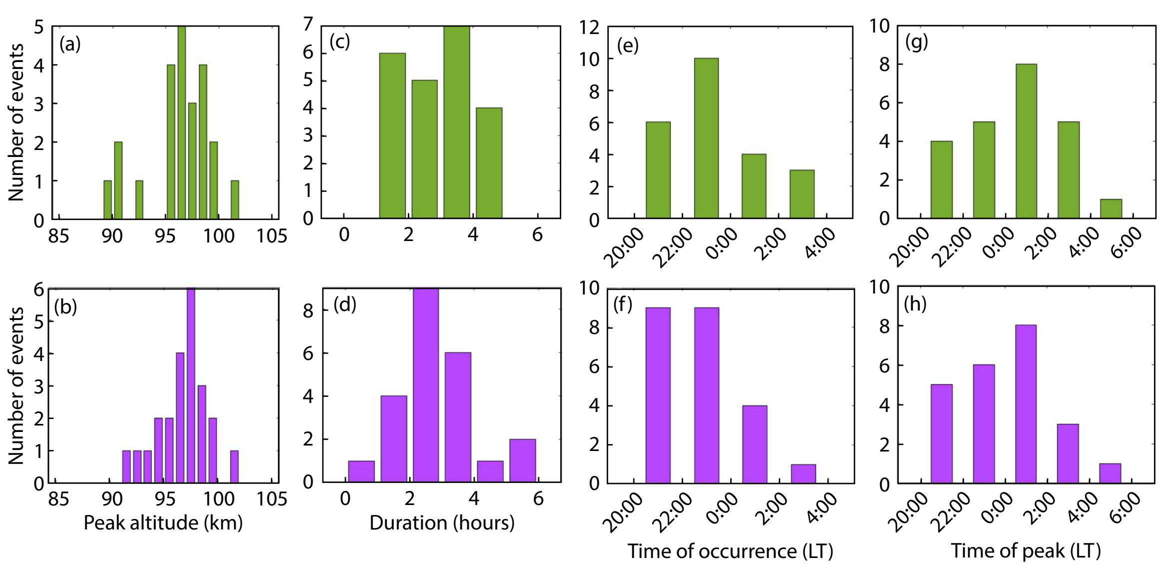

Figure 6. Histogram of peak altitude, duration, time of occurrence, and peak time of 23 simultaneous Nis and Nas. The top row represents Nis (green columns) and the bottom row represents Nas (purple columns). Panels (a) and (b) show the peak altitude, panels (c) and (d) represent the duration, panels (e) and (f) show the time of occurrence, and panels (g) and (h) represent the peak time.

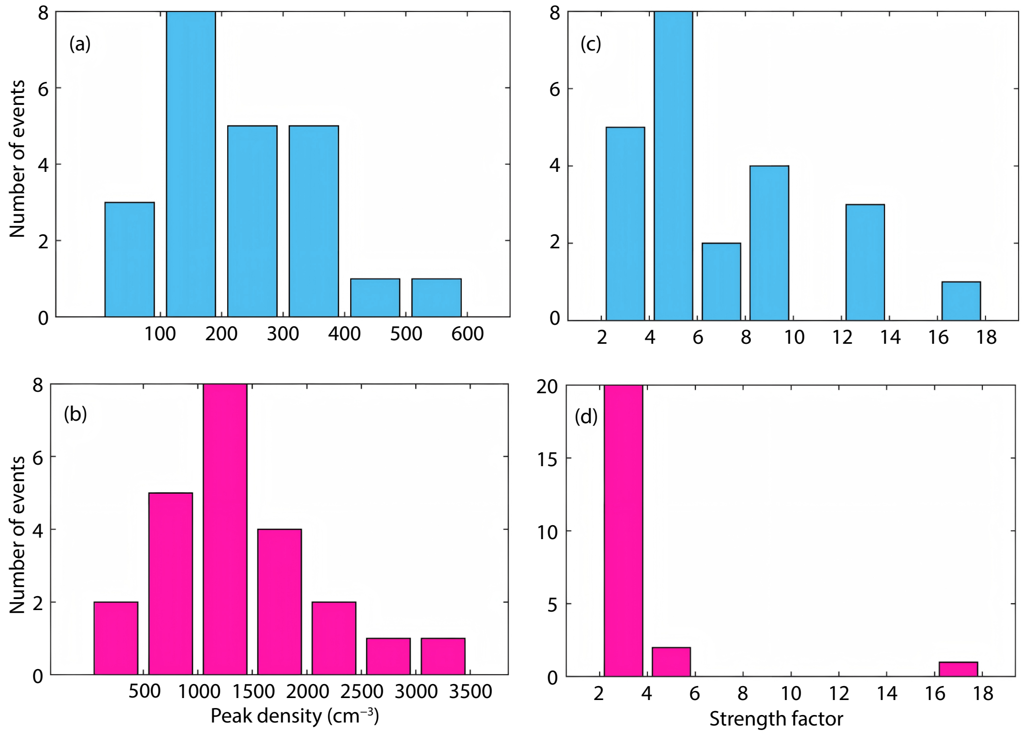

Figure 7. Histogram of peak density and strength factors of 23 simultaneous Nis and Nas. The top row represents Nis (blue columns) and the bottom row represents Nas (pink columns). Panels (a) and (b) present the peak density distributions, and panels (c) and (d) illustrate the strength factor characteristics.

mum value between 100 and 200 cm^{-3}, whereas the peak density of Nas is significantly higher, with a maximum value between 1000 and 1500 cm^{-3}. As a whole, the peak density of Nas is approximately 5–6 times that of Nis. Furthermore, Figures 7c and 7d show the strength factor distributions for both Nis and Nas. It is clear that the strength factor of Nis is significantly larger than that of Nas and that the Nis is mainly concentrated in the intensity factor range of 4–6. In contrast, the strength factor of Nas is generally lower, mainly in the range of 2 to 4. This difference may be attributed to the higher background density of the Na layer.

In conclusion, the changes in density and morphological structure of these 23 Nis and Nas are similar. However, the strength factor of Nis is larger than that of Nas, and the peak density ratio of Nas to Nis is approximately 5, which is half the density ratio of the two main layers. This result indicates that Ni is relatively enriched relative to the main layer.

4. Discussion

Extensive Na lidar observations and model simulations have consistently demonstrated that the primary reservoir of Nas originates from Na^+ in the Es layer, where the thin layer near the upper boundary of the Na layer undergoes neutralization, forming an enhanced Na atom layer (Cox and Plane, 1998; Andrioli et al., 2020, 2024; Pimenta et al., 2022). Currently, Es theory has been widely accepted. Thus, we use the digital ionospheric sounding data from the Beijing Shisanling station to analyze the relationship between Nis and Nas and Es, and we discuss the influence of Ni^+/Na^+ neutralization in Es on the formation of Nis and Nas from the perspective of chemical reactions. These Es data are all within the time range of valid data for the Ni atomic layer.

4.1 Correlation Between Nis and Nas and Es

We analyzed the Es data during the effective observation period of the lidar. Figure 8a shows the monthly average occurrence frequencies of Nis, Nas, and Es. We can see that both Nis and Nas and Es occur more frequently in summer. Our analysis found a positive correlation between the average monthly occurrence of Nis and Nas and that of Es, and the correlation coefficient is approximately 0.7. In addition, the frequency of occurrence of Nis and Nas is the highest in June and July, whereas Es does not exhibit this feature. The Es layer has the highest frequency of occurrence in May and August. At this time, the frequency of occurrence of Nis and Nas is less than those in June and July. This result indicates that when Es emerges, Nis and Nas does not necessarily occur. This characteristic may be related to multiple factors. In terms of chemical reactions, sometimes the strength of Es is relatively low, the content of metal ions in Es is low, and the number of metal atoms produced by the neutralization of metal ions is very small, to the extent that it does not meet our screening criteria for Nis and Nas. Therefore, we conducted a further analysis of the relationship between f_oEs (the critical frequency of the sporadic E layer) and the Nis and Nas strength factor. Figure 8b presents the monthly average strength factor of Nis and Nas and the monthly average f_oEs. The strength factor of Nis and Nas increases with the growth of the f_oEs, showing a relatively consistent trend in which both peak during June and July. These results further indicate that Nis, Nas, and Es show good consistency in seasonal variation.

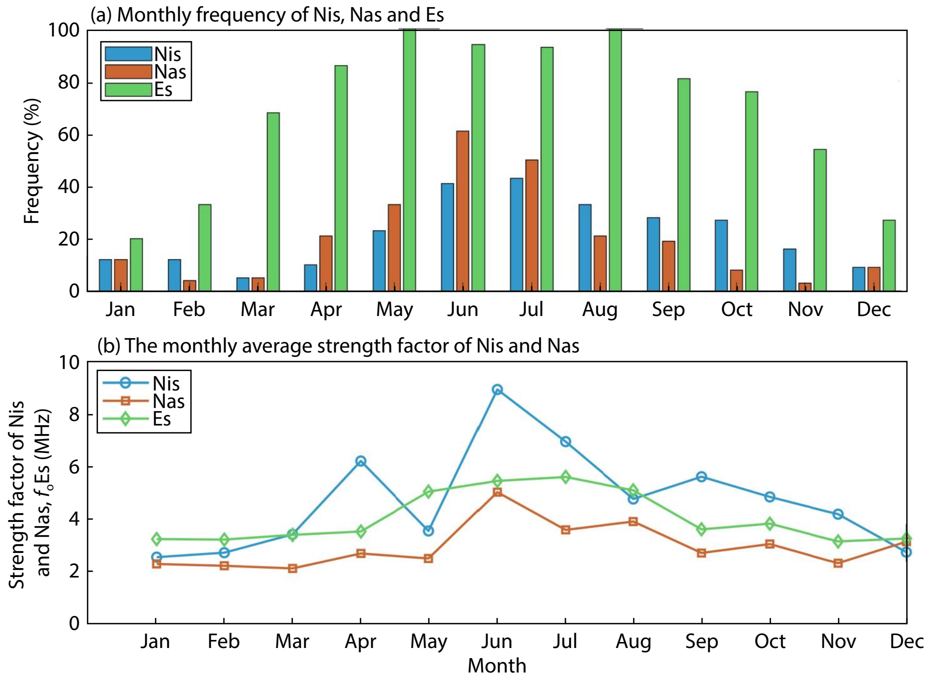

Figure 8. (a) The monthly frequency of Nis and Nas and Es; (b) the monthly average strength factor of Nis and Nas and the monthly average f_oEs.

Among the 69 observed Nis events, 54 events (79%) occur on nights accompanied by Es, whereas among the 56 Nas events, a corresponding Es is observed in 46 events (82%). Further analysis revealed that among the 54 Nis accompanied by Es, Es appears first in 74% (40 Nis) of the events. Among the 46 Nas events associated with Es, Es occur before the corresponding Nas in 83% (38 Nas) of the events. Figure 9 shows the appearance times of 40 Nis and 38 Nas and the corresponding Es. Note that variation trends in the times of occurrence of Nis and Nas and Es are largely consistent, with the time difference between them remaining within 3 h.

Figure 10 shows the peak altitude of Nis and Nas, along with the corresponding virtual height of the Es layer (*h*'Es). Statistical results indicated that Nis and Nas exhibit a significant correlation with Es in terms of height variations. These results illustrate that a good correlation exists between Nis and Nas and Es.

4.2 Discussion of Ni^+/Na^+ Neutralization in Es

Previous studies have shown that below 100 km, the neutralization of metal ions mainly occurs through dissociation recombination reactions (Plane, 2004; Jiao J et al., 2022; Wu FJ et al., 2022).

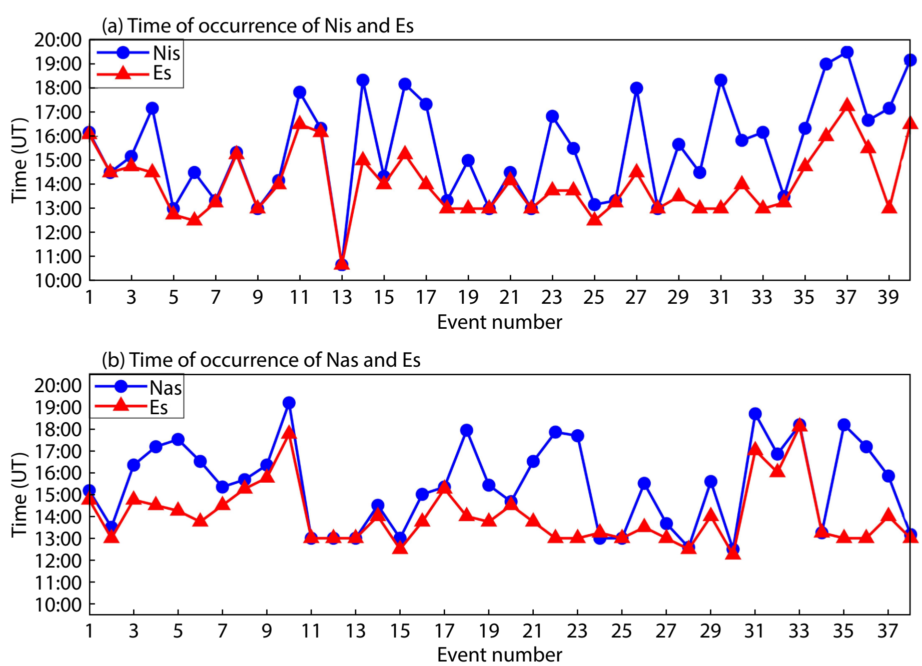

Figure 9. The times of occurrence of 54 Nis, 46 Nas, and Es.

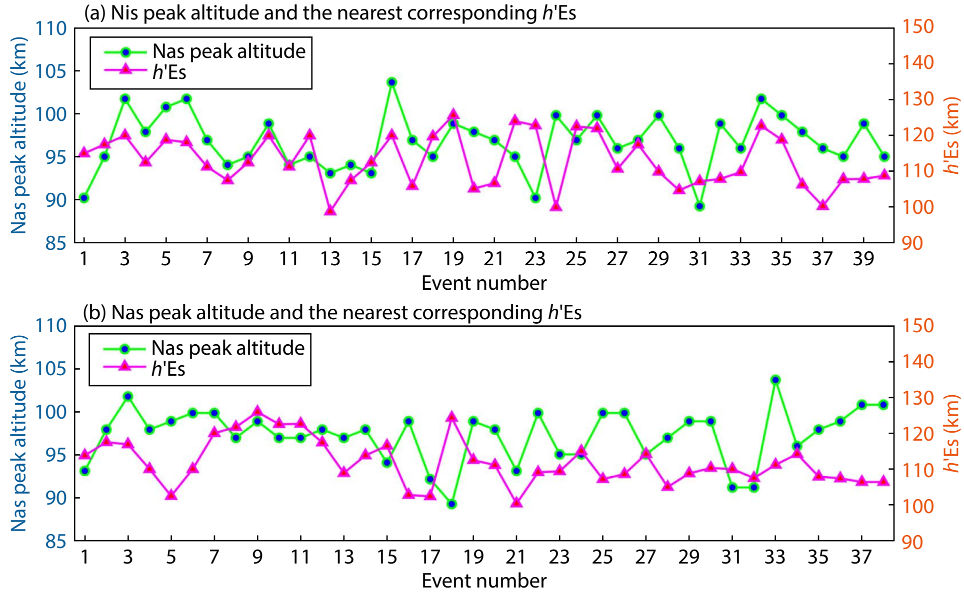

Figure 10. The peak altitude of Nis and Nas and the nearest corresponding virtual height of the Es layer (*h*'Es).

Tables 3 and 4, respectively, present the dissociation recombination reactions of Ni^+ and Na^+ (Plane et al., 2015; Daly et al., 2020). The means of dissociative recombination for Ni^+ and Na^+ are different. The Ni ion reacts with O_3 and O_2 to form stable nickel oxide ions, which subsequently undergo dissociative recombination with electrons. However, Na^+ first associates with N_2 and CO_2

Table 3. The dissociation recombination reactions of Ni^+ and rate coefficients.

No.	Reaction	Rate coefficient[a]
1	$Ni^+ + O_3 \rightarrow NiO^+ + O_2$	$9.8\times10^{-10}\exp(T/294\ K)$
2	$Ni^+ + O_2\ (+ M = N_2\ \&\ O_2) \rightarrow NiO_2^+$	$\log_{10}(K) = -27.8098 + 1.3065\log_{10}(T) - 0.81136[\log_{10}(T)]^2$
4	$NiO^+ + O \rightarrow Ni^+ + O_2$	1.7×10^{-10}
5	$Ni^+\cdot N_2 + O \rightarrow NiO^+ + N_2$	7×10^{-12}
6	$NiO_2^+ + O \rightarrow NiO^+ + O_2$	5×10^{-11}
7	$NiO^+ + e^- \rightarrow Ni + O$	$5.5\times10^{-7}\ (300\ K/T)^{0.5}$
8	$NiO_2^+ + e^- \rightarrow Ni + O_2$	$3\times10^{-7}\ (200\ K/T)^{0.5}$
9	$Ni^+\cdot N_2 + e^- \rightarrow Ni + N_2$	$3\times10^{-7}\ (200\ K/T)^{0.5}$

[a] Units for bimolecular reactions: cubic centimeters per molecule per second. *T* is temperature, K is a unit of temperature.

Table 4. The dissociation recombination reactions of Na^+ and rate coefficients.

No.	Reaction	Rate coefficient[a]
1	$Na^+ + N_2\ (+ M = N_2\ \&\ O_2) \rightarrow Na^+\cdot N_2$	$4.8\times10^{-30}\ (T/200\ K)^{-2.2}$
2	$Na^+ + CO_2\ (+ M) \rightarrow Na^+\cdot CO_2$	$3.7\times10^{-29}\ (T/200\ K)^{-2.84}$
3	$Na^+\cdot N_2 + CO_2 \rightarrow Na^+\cdot CO_2 + N_2$	6×10^{-10}
4	$Na^+\cdot N_2 + O \rightarrow NaO^+ + N_2$	4×10^{-10}
5	$NaO^+ + O \rightarrow Na^+ + O_2$	1×10^{-11}
6	$NaO^+ + N_2 \rightarrow Na^+\cdot N_2 + O$	1×10^{-12}
7	$NaO^+ + O_2 \rightarrow Na^+ + O_3$	5×10^{-12}
8	$NaO^+ + CO_2 \rightarrow Na^+\cdot CO_2 + O$	6×10^{-10}
9	$Na^+\cdot X\ (X = O, N_2, CO_2) + e^- \rightarrow Na + X$	$1\times10^{-6}\ (200\ K/T)^{0.5}$

[a] Units for bimolecular reactions: cubic centimeters per molecule per second.

molecules to form cluster ions, which then undergo dissociative recombination with electrons to produce Na.

We found, based on statistical analysis of the monthly average f_oEs, that from May to August, $f_o\text{Es} \geq 5$ MHz appears with the large strength factor of Nis and Nas. Therefore, according to the aforementioned chemical reactions, we calculated the neutralization rate of Ni^+ and Na^+ at altitudes of 90–100 km for $f_o\text{Es} = 5$ MHz by using the WACCM-Ni model (as shown in Figure 11). Below 98 km, the neutralization rate of Ni^+ is lower than that of Na^+. However, the disparity between them is notably smaller than that displayed in Figure 11 of Jiao J et al. (2022). This difference occurs because the Es layers provide enhanced electron and Ni^+ densities, accelerating Ni^+ neutralization; hence, the observed relative abundance of Ni is higher in sporadic layers compared with the main layer.

According to the statistical results for Nis and Nas, the peak heights of Nis are mainly distributed around 95 km (as shown in Figures 6 and 10). At 95 km, the neutralization rate for Ni^+ is approximately 1×10^{-4} (s^{-1}), whereas for Na^+ it is approximately 2×10^{-4} (s^{-1}). Thus, the neutralization rate for Na^+ is approximately twice that of Ni^+. Furthermore, Wu FJ et al. (2022) reported that at an f_oEs of 5 MHz, the concentrations of Ni^+ and Na^+ within Es layers are 6×10^3 cm^{-1} and 1.3×10^4 cm^{-1}, respectively. This result indicates that the Na^+ concentration is 2.2 times that of Ni^+. According to the analysis above, the ratio of the Ni production rate to the Na production rate is estimated to be 1:4.4, which closely aligns with our statistical density ratio of Nis to Nas (1:5). Therefore, the neutralization reaction of Ni^+, Na^+, and electrons in Es is the main reason for the formation of the Nis layer and the Nas layer.

5. Conclusion

In this article, we analyzed 343 nights of lidar data from April 2019 to October 2022 by using simultaneous lidar observations of Ni and Na at the Yanqing station in Beijing. According to our selection criteria, 68 Nis and 56 Nas were recorded. We conducted a statistical analysis of the seasonal variations of Nis and Nas. The results revealed that both Nis and Nas occur more frequently in summer than in winter: Nis occurs the most frequently in July, and Nas has its greatest occurrence in June. In addition, we identified 23 events in which Nis and Nas occur simultaneously.

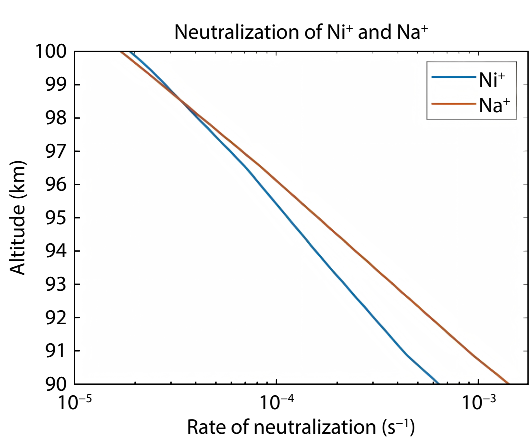

Figure 11. Variation in the neutralization rate of Ni^+ and Na^+ with altitude.

We compared and analyzed the characteristic parameters of these 23 events. The results indicated that the average peak altitude of Nis is approximately 1 km lower than that of Nas. The duration of Nis and Nas is almost 1 h or more. Meanwhile, we also observed that Nis and Nas appear mainly before midnight, and they tend to peak at 00:00–02:00 LT. In general, Nis and Nas have similar change characteristics. We discovered, based on a statistical analysis of the peak density, that the peak density ratio of Nis to Nas is approximately 1:5. However, the peak density ratio of the main Ni layer to the main Na layer is approximately 1:10, which indicates that Ni is fairly enriched relative to the main layer. The Nis strength factor is greater than 4, whereas the Nas strength factor is mainly between 2 and 4. This difference may be due to the greater density of the background Na layer.

Through comparative analysis of simultaneous Es data, we found a significant correlation between the monthly mean frequency of occurrence of Nis and Nas and Es (correlation coefficient of ~0.7). Furthermore, the variation trends of the f_oEs and Nis and Nas strength factors are similar. Further analysis of the correspondence between individual Nis and Nas events and Es indicated that approximately 79% of Nis (82% of Nas) events occur accompanied by Es. This result demonstrates a high correlation between Nis and Nas and Es. On the basis of calculations of the dissociation recombination reactions of Ni ions and the WACCM-Ni model, we obtained the neutralization rates of Ni^+ and Na^+ when f_oEs is 5 MHz and estimated the ratio of the Ni production rate to Na production rate as approximately 1:4.4. This ratio closely matches the density ratio of Nis to Nas obtained from our statistical analysis. These results show that dissociative recombination reactions of Ni^+ and Na^+ with electrons in the Es layers serve as the primary formation mechanism for Nis and Nas.

By analyzing the lidar data, we performed a more systematic analysis of Nis and Nas and analyzed their connection to Es. However, some questions regarding the detailed chemical reaction process between Nis and Nas and Es remain unresolved. More observational and simulation studies are necessary to explore these questions.

Authorship contribution statement

Zhijun Zhao: Validation, methodology, software, writing–review.
Xuyang Jiang: Investigation, data processing, software, writing–original draft, writing–review and editing.
Fuju Wu: Resources, data curation, validation, investigation, methodology, writing–review and editing, funding acquisition.
Yuhang Qi: Investigation, software, data processing.
Jing Jiao: Formal analysis, visualization.
Guotao Yang: Resources, data curation, supervision.

Data Availability Statement

Sporadic E data were provided by the Beijing Space Environment Observatory, Institute of Geology and Geophysics, Chinese Academy of Sciences, through the Center for Geophysics and the National Earth System Science Data Center (http://wdc.geophys.ac.cn). The data presented in this study can be downloaded from the Dryad data repository (https://doi.org/10.5061/dryad.47d7wm3r7).

Declarations

All authors consent to publication.
The authors declare no competing interests.

Acknowledgments

This work was supported by the Specialized Research Fund for State Key Laboratories, Chinese Meridian Project, the Specialized Research Fund for the State Key Laboratory of Solar Activity and Space Weather, postgraduate Education Reform and Quality Improvement Project of Henan Province (Grant No. YJS2024JD32), Natural Science Foundation Project of Henan Province (Grant No. 242300420253), and National Natural Science Foundation of China for Young Scientists (Grant No. 42504156) funding.

References

Andrioli, V. F., Xu, J., Batista, P. P., Pimenta, A. A., Resende, L. C. A., Savio, S., Fagundes, P. R., Yang, G., Jiao, J., … Liu, Z. (2020). Nocturnal and seasonal variation of Na and K layers simultaneously observed in the MLT region at 23°S. *J. Geophys. Res.: Space Phys.*, *125*(3), e2019JA027164. https://doi.org/10.1029/2019JA027164

Andrioli, V. F., Xu, J. Y, Batista, P. P., Resende, L. C. A., Da Silva, L. A., Pimenta, A. A., Martins, M. P. P., Santos, A. M., Moro, J., … Liu, Z. K. (2024). Peculiar enhancement in the neutral K and Na layers observed during atypical E-region event in the South American magnetic anomaly (SAMA) region. *Front. Astron. Space Sci.*, *11*, 1458148. https://doi.org/10.3389/fspas.2024.1458148

Bowman, M. R., Gibson, A. J., and Sandford, M. C. W. (1969). Atmospheric sodium measured by a tuned laser radar. *Nature*, *221*(5179), 456–457. https://doi.org/10.1038/221456a0

Cai, X. G., Yuan, T., and Eccles, J. V. (2017). A numerical investigation on tidal and gravity wave contributions to the summer time Na variations in the midlatitude E region. *J. Geophys. Res.: Space Phys.*, *122*(10), 10577–10595. https://doi.org/10.1002/2016JA023764

Chu, X. Z., and Papen, G. (2005). Resonance fluorescence lidar for measurements of the middle and upper atmosphere. In T. Fujii and T. Fukuchi (Eds.), *Laser Remote Sensing* (pp. 179–432). Boca Raton, FL: CRC Press. https://doi.org/10.1201/9781420030754.ch5

Clemesha, B. R., Kirchhoff, V. W. J. H., Simonich, D. M., and Takahashi, H. (1978). Evidence of an extra-terrestrial source for the mesospheric sodium layer. *Geophys. Res. Lett.*, *5*(10), 873–876. https://doi.org/10.1029/GL005i010p00873

Collins, R. L., Li, J., and Martus, C. M. (2015). First lidar observation of the mesospheric nickel layer. *Geophys. Res. Lett.*, *42*(2), 665–671. https://doi.org/10.1002/2014gl062716

Cox, R. M., and Plane, J. M. C. (1998). An ion-molecule mechanism for the formation of neutral sporadic Na layers. *J. Geophys. Res.: Atmos.*, *103*(D6), 6349–6359. https://doi.org/10.1029/97JD03376

Daly, S. M., Feng, W. H., Mangan, T. P., Gerding, M., and Plane, J. M. C. (2020). The meteoric Ni layer in the upper atmosphere. *J. Geophys. Res.: Space Phys.*, *125*(8), e2020JA028083. https://doi.org/10.1029/2020JA028083

Dou, X. K., Qiu, S. C., Xue, X. H., Chen, T. D., and Ning, B. Q. (2013). Sporadic and thermospheric enhanced sodium layers observed by a lidar chain over China. *J. Geophys. Res.: Space Phys.*, *118*(10), 6627–6643. https://doi.org/10.1002/jgra.50579

Gardner, C. S., Chu, X. Z., Espy, P. J., Plane, J. M. C., Marsh, D. R., and Janches, D. (2011). Seasonal variations of the mesospheric Fe layer at Rothera, Antarctica (67.5°S, 68.0°W). *J. Geophys. Res.: Atmos.*, *116*(D2), D02304. https://doi.org/10.1029/2010JD014655

Gerding, M., Daly, S., and Plane, J. M. C. (2019). Lidar soundings of the mesospheric nickel layer using $Ni(^3F)$ and $Ni(^3D)$ transitions. *Geophys. Res. Lett.*, *46*(1), 408–415. https://doi.org/10.1029/2018GL080701

He, S. M., Zhang, T. M., Chai, W. W., Zhang, Y. M., Yang, D. L., Peng, H. Y., and Wang, J. H. (2025). Seasonal variation characteristics of sodium layer in low latitude by lidar. *Chin. J. Space Sci. (in Chinese)*, *45*(1), 102–112. https://doi.org/10.11728/cjss2025.01.2024-0035

Hu, Y. J., and Yi, F. (2021). Structures and interannual variations of the nocturnal mesospheric Na and Fe layers at 30°N. *Chin. J. Space Sci. (in Chinese)*, *41*(2), 279–285. https://doi.org/10.11728/cjss2021.02.279

Jiao, J., Yang, G. T., Zou, X., Gong, S. H., Wang, J. H., Tian, D. W., Zhang, W. Z., Zhang, T. M., Yang, X. C., … Cheng, X. W. (2014). Joint observations of sporadic sodium and sporadic E layers at middle and low latitudes in China. *Chin. Sci. Bull.*, *59*(29), 3868–3876. https://doi.org/10.1007/s11434-014-0441-0

Jiao, J., Yang, G. T., Wang, J. H., Cheng, X. W., Li, F. Q., Yang, Y., Gong, W., Wang, Z. L., Du, L. F., … Gong, S. S. (2015). First report of sporadic *K* layers and comparison with sporadic Na layers at Beijing, China (40.6°N, 116.2°E). *J. Geophys. Res.: Space Phys.*, *120*(6), 5214–5225. https://doi.org/10.1002/2014JA020955

Jiao, J., Feng, W. H., Wu, F., Wu, F. J., Zheng, H. R., Du, L. F., Yang, G. T., and Plane, J. (2022). A comparison of the midlatitude nickel and sodium layers in the mesosphere: Observations and modeling. *J. Geophys. Res.: Space Phys.*, *127*(2), e2021JA030170. https://doi.org/10.1029/2021JA030170

Ma, Z., Wang, X., Chen, L., and Wu, J. (2014). First report of sporadic Na layers at Qingdao (36°N, 120°E), China. *Ann. Geophys.*, *32*(7), 739–748. https://doi.org/10.5194/angeo-32-739-2014

Pimenta, A. A., Batista, P. P., Andrioli, V. F., Fagundes, P. R., and Batista, I. S. (2022). Possible relationship of meteor disintegration in the mesosphere and enhancement of sodium atoms: A case study on July 05, 2013. *Adv. Space Res.*, *69*(3), 1344–1350. https://doi.org/10.1016/j.asr.2021.11.028

Plane, J. M. C., Gardner, C. S., Yu, J. R., She, C. Y., Garcia, R. R., and Pumphrey, H. C. (1999). Mesospheric Na layer at 40°N: Modeling and observations. *J. Geophys. Res.: Atmos.*, *104*(D3), 3773–3788. https://doi.org/10.1029/1998JD100015

Plane, J. M. C. (2004). A time-resolved model of the mesospheric Na layer: Constraints on the meteor input function. *Atmos. Chem. Phys.*, *4*(3), 627–638. https://doi.org/10.5194/acp-4-627-2004

Plane, J. M. C., Feng, W. H., and Dawkins, E. C. M. (2015). The mesosphere and metals: Chemistry and changes. *Chem. Rev.*, *115*(10), 4497–4541. https://doi.org/10.1021/cr500501m

Qiu, S. C., Tang, Y. H., Jia, M. J., Xue, X. H., Dou, X. K., Li, T., and Wang, Y. H. (2016). A review of latitudinal characteristics of sporadic sodium layers, including new results from the Chinese Meridian Project. *Earth-Sci. Rev.*, *162*, 83–106. https://doi.org/10.1016/j.earscirev.2016.07.004

Qiu, S. C., Soon, W., Xue, X. H., Li, T., Wang, W. Y., Jia, M. J., Ban, C., Fang, X., Tang, Y. H., and Dou, X. K. (2018). Sudden sodium layers: Their appearance and disappearance. *J. Geophys. Res.: Space Phys.*, *123*(6), 5102–5118. https://doi.org/10.1029/2017JA024883

Qiu, S. C., Wang, N., Soon, W., Lu, G. P., Jia, M. J., Wang, X. J., Xue, X. H., Li, T., and Dou, X. K. (2021). The sporadic sodium layer: A possible tracer for the conjunction between the upper and lower atmospheres. *Atmos. Chem. Phys.*, *21*(15), 11927–11940. https://doi.org/10.5194/acp-21-11927-2021

Qiu, S. C., Shi, M. X., Yousof, H., Soon, W., Jia, M. J., Xue, X. H., Li, T., Ju, P., and Dou, X. K. (2023). Solitary wave characteristics on the fine structure of the mesospheric sporadic sodium layer. *Front. Astron. Space Sci.*, *10*, 1241663. https://doi.org/10.3389/fspas.2023.1241663

Raizada, S., Tepley, C. A., Aponte, N., and Cabassa, E. (2011). Characteristics of neutral calcium and Ca^+ near the mesopause, and their relationship with sporadic ion/electron layers at Arecibo. *Geophys. Res. Lett.*, *38*(9), L09103. https://doi.org/10.1029/2011GL047327

Raizada, S., Smith, J. A., Lautenbach, J., Aponte, N., Perillat, P., Sulzer, M., and Mathews, J. D. (2020). New lidar observations of Ca^+ in the mesosphere and lower thermosphere over Arecibo. *Geophys. Res. Lett.*, *47*(5), e2020GL087113. https://doi.org/10.1029/2020GL087113

Takahashi, T., Nozawa, S., Tsuda, T. T., Ogawa, Y., Saito, N., Hidemori, T., Kawahara, T. D., Hall, C., Fujiwara, H., … Fujii, R. (2015). A case study on generation mechanisms of a sporadic sodium layer above Tromsø (69.6° N) during a night of high auroral activity. *Ann. Geophys.*, *33*(8), 941–953. https://doi.org/10.5194/angeo-33-941-2015

Von Zahn, U., Von der Gathen, P., and Hansen, G. (1987). Forced release of sodium from upper atmospheric dust particles. *Geophys. Res. Lett.*, *14*(1), 76–79. https://doi.org/10.1029/GL014i001p00076

Wang, Z. L., Yang, G. T., Wang, J. H., Yue, C., Yang, Y., Jiao, J., Du, L. F., Cheng, X. W., and Chi, W. (2017). Seasonal variations of meteoric potassium layer over Beijing (40.41°N, 116.01°E). *J. Geophys. Res.: Space Phys.*, *122*(2), 2016–2118. https://doi.org/10.1002/2016JA023216

Wu, F. J., Zheng, H. R., Yang, Y., Cheng, X. W., Li, F. Q., Du, L. F., Wang, J. H., Jiao, J., Plane, J. M. C., … Yang, G. T. (2021). Lidar observations of the upper atmospheric nickel layer at Beijing (40°N, 116°E). *J. Quant. Spectrosc. Radiat. Transfer.*, *260*, 107468. https://doi.org/10.1016/j.jqsrt.2020.107468

Wu, F. J., Chu, X. Z., Du, L. F., Jiao, J., Zheng, H. R., Xun, Y. C., Feng, W. H., Plane, J. M. C., and Yang, G. T. (2022). First simultaneous lidar observations of thermosphere–ionosphere sporadic Ni and Na (TISNi and TISNa) Layers (~105–120 km) over Beijing (40.42°N, 116.02°E). *Geophys. Res. Lett.*, *49*(16), e2022GL100397. https://doi.org/10.1029/2022GL100397

Wu, F., Jiao, J., Yang, G. T., Du, L. F., Liu, Z. K., Zheng, H. R., Guo, J. X., Gong, S. H., and Zhu, Y. J. (2025). The low-latitude sodium layer: comparative data from lidar observations at Hainan, China and São Paulo, Brazil. *Earth Planet. Phys.*, *9*(1), 39–53. https://doi.org/10.26464/epp2024014

Xia, Y., Cheng, X. W., Li, F. Q., Yang, Y., Lin, X., Jiao, J., Du, L. F., Wang, J. H., and Yang, G. T. (2020). Sodium lidar observation over full diurnal cycles in Beijing, China. *Appl. Opt.*, *59*(6), 1529–1536. https://doi.org/10.1364/AO.382077

Xun, Y. C., Zhao, P., Wang, Z. L., Du, L. F., Jiao, J., Chen, Z. S., Zheng, H. R., Gong, S. H., and Yang, G. T. (2024). Seasonal variation in the mesospheric Ca layer and Ca^+ layer simultaneously observed over Beijing (40.41°N, 116.01°E). *Remote Sens.*, *16*(3), 596. https://doi.org/10.3390/rs16030596

Yi, F., Zhang, S. D., Zeng, H. J., He, Y. J., Yue, X. C., Liu, J. B., Lv, H. F., and Xiong, D. H. (2002). Lidar observations of sporadic Na layers over Wuhan (30.5°N, 114.4°E). *Geophys. Res. Lett., 29*(9), 59-1–59-4. https://doi.org/10.1029/2001GL014353

Yi, F., Zhang, S. D., Yu, C. M., He, Y. J., Yue, X. C., Huang, C. M., and Zhou, J. (2007). Simultaneous observations of sporadic Fe and Na layers by two closely colocated resonance fluorescence lidars at Wuhan (30.5°N, 114.4°E), China. *J. Geophys. Res.: Atmos.*, *112*(D4), D04303. https://doi.org/10.1029/2006JD007413

Yuan, T., Wang, J. H., Cai, X. G., Sojka, J., Rice, D., Oberheide, J., and Criddle, N. (2014). Investigation of the seasonal and local time variations of the high-altitude sporadic Na layer (Na_S) formation and the associated midlatitude descending *E* layer (E_s) in lower *E* region. *J. Geophys. Res.: Space Phys.*, *119*(7), 5985–5999. https://doi.org/10.1002/2014JA019942

Yuan, T., Stevens, M. H., Englert, C. R., and Immel, T. J. (2021). Temperature tides across the mid-latitude summer turbopause measured by a sodium lidar and MIGHTI/ICON. *J. Geophys. Res.: Atmos.*, *126*(16), e2021JD035321. https://doi.org/10.1029/2021JD035321

Zhang, T. M., Wang, J. H., Wang, L. M., Chen, X. M., Wu, J. Q., Zou, X., and Peng, H. Y. (2017). Observations of sodium layer over Beijing and Haikou in July 2012. *Chin. J. Space Sci. (in Chinese)*, *37*(4), 424–431. https://doi.org/10.11728/cjss2017.04.424